Journal of Structural Biology 189 (2015) 220–229

Contents lists available at ScienceDirect

Journal of Structural Biology

journal homepage: www.elsevier.com/locate/yjsbi

Cryo-electron tomography of plunge-frozen whole bacteria and vitreous sections to analyze the recently described bacterial cytoplasmic structure, the Stack

Lidia Delgado [a,b], Gema Martínez [a], Carmen López-Iglesias [a,*], Elena Mercadé [b,*]

[a] Cryo-Electron Microscopy, Scientific and Technological Centers, University of Barcelona, Barcelona, Spain
[b] Department of Microbiology, Faculty of Pharmacy, University of Barcelona, Barcelona, Spain

ARTICLE INFO

Article history:
Received 12 December 2014
Accepted 13 January 2015
Available online 21 January 2015

Keywords:
Cryo-electron microscopy
Cryo-electron tomography
Vitreous sections
Plunge freezing
High-pressure freezing
Stacks

ABSTRACT

Cryo-electron tomography (CET) of plunge-frozen whole bacteria and vitreous sections (CETOVIS) were used to revise and expand the structural knowledge of the "Stack", a recently described cytoplasmic structure in the Antarctic bacterium *Pseudomonas deceptionensis* M1^T. The advantages of both techniques can be complementarily combined to obtain more reliable insights into cells and their components with three-dimensional imaging at different resolutions. Cryo-electron microscopy (Cryo-EM) and CET of frozen-hydrated *P. deceptionensis* M1^T cells confirmed that Stacks are found at different locations within the cell cytoplasm, in variable number, separately or grouped together, very close to the plasma membrane (PM) and oriented at different angles (from 35° to 90°) to the PM, thus establishing that they were not artifacts of the previous sample preparation methods. CET of plunge-frozen whole bacteria and vitreous sections verified that each Stack consisted of a pile of oval disc-like subunits, each disc being surrounded by a lipid bilayer membrane and separated from each other by a constant distance with a mean value of 5.2 ± 1.3 nm. FM4-64 staining and confocal microscopy corroborated the lipid nature of the membrane of the Stacked discs. Stacks did not appear to be invaginations of the PM because no continuity between both membranes was visible when whole bacteria were analyzed. We are still far from deciphering the function of these new structures, but a first experimental attempt links the Stacks with a given phase of the cell replication process.

1. Introduction

In the last years, advances in transmission electron microscopy (TEM) have enhanced our knowledge of bacterial ultrastructure (Chang et al., 2014; Hoenger, 2014; Comolli et al., 2011, 2013; Milne et al., 2013; Basler et al., 2012; Gan and Jensen, 2012; Chen et al., 2010; Sani et al., 2010; Tocheva et al., 2010; Li and Jensen, 2009; Milne and Subramaniam, 2009; Jensen and Briegel, 2007). Cryo-electron microscopy (Cryo-EM) combined with tomography has allowed already known structures to be visualized in a close-to-native state, providing the highest resolution available for the imaging of biological specimens. These "pure" cryo-techniques have revealed cellular organelles and macromolecular assemblies in a frozen-hydrated state, avoiding contrast-enhancing staining solutions, chemical fixatives and resins, which may contaminate the sample with artifacts. One way to obtain the cooling rates required for water vitrification is plunge freezing, after which 'whole-mount' plunge-frozen specimens can be imaged directly when their thickness is below 0.5 μm, a range that includes many bacteria and archaea (Beeby et al., 2012; Toso et al., 2011; Kudryashev et al., 2010; Comolli et al., 2006, 2008; Khursigara et al., 2008; Murphy et al., 2008; Li et al., 2007; Zhang et al., 2007; Briegel et al., 2006; Komeili et al., 2006; Scheffel et al., 2006). However, the resolution of Cryo-EM of plunge-frozen whole bacteria is conditioned by the thickness of the sample, limiting the

Abbreviations: CET, cryo-electron tomography; CEMOVIS, cryo-electron microscopy of vitreous sections; CETOVIS, cryo-electron tomography of vitreous sections; Cryo-EM, cryo-electron microscopy; HPF, high-pressure freezing; FS, freeze substitution; LN_2, liquid nitrogen; PM, plasma membrane; TEM, transmission electron microscopy; VIS, vitreous sections.

* Corresponding authors at: Crio-Microscòpia Electrònica, Centres Científics i Tecnològics, Universitat de Barcelona, C. Baldiri i Reixac, 10-12, E-08028 Barcelona, Spain. Fax: +34 934039037 (C. López-Iglesias). Departament de Microbiologia i Parasitologia Sanitàries, Facultat de Farmàcia, Universitat de Barcelona, Av. Juan XXIII s/n, E-08028 Barcelona, Spain. Fax: +34 934024498 (E. Mercadé).

E-mail addresses: carmenli@ccit.ub.edu (C. López-Iglesias), mmercade@ub.edu (E. Mercadé).

http://dx.doi.org/10.1016/j.jsb.2015.01.008
1047-8477/

observation of molecular details. Cryo-electron microscopy of vitreous sections (CEMOVIS) is an alternative technique to study frozen-hydrated bacteria, consisting of obtaining thin sections from cryoimmobilized whole bacteria, which provide a better resolution than plunge-frozen whole bacteria. To achieve thin sections, high-pressure freezing (HPF) provides vitrification of the samples up to 200 μm by increasing the pressure to 2048 bars during the cooling (Studer et al., 2008). Ultrathin sections of 50 nm can be directly obtained from high-pressure frozen bacteria and imaged in the microscope, disclosing molecular details such as the lipid bilayer membrane (Hoffmann et al., 2008; Zuber et al., 2008). However, it is important to bear in mind that the mechanical action of cutting can add conspicuous artifacts to the sample (Al-Amoudi et al., 2005).

Frozen-hydrated specimens can be processed by cryo-electron tomography (CET), performed by incrementally tilting the sample in the Cryo-EM through a range up to ±70 and imaged at each step. Afterwards, the tilt series of images is aligned and processed to generate a 3D reconstruction or tomogram of the specimen. CET has been applied to already known structural assemblies such as layers of the bacterial cell envelope (Kishimoto-Okada et al., 2010; Hoffmann et al., 2008; Zuber et al., 2008; Al-Amoudi et al., 2004), chemoreceptors (Briegel et al., 2008; Khursigara et al., 2008; Zhang et al., 2007), cytoskeleton filaments (Pilhofer et al., 2011; Ingerson-Mahar et al., 2010; Salje et al., 2009; Li et al., 2007; Briegel et al., 2006; Komeili et al., 2006; Scheffel et al., 2006; Kürner et al., 2005; Erickson, 1997), flagella (Chen et al., 2011; Kudryashev et al., 2010; Liu et al., 2009; Murphy et al., 2008), magnetosomes (Komeili et al., 2006; Scheffel et al., 2006), storage granules (Beeby et al., 2012; Hoenger and McIntosh, 2009; Comolli et al., 2006), carboxysomes (Iancu et al., 2010) and the Type VI secretion system (Chang et al., 2014), providing new information and a greater understanding of those structures in their natural context. Furthermore, the use of Cryo-EM and CET has led to the discovery of new bacterial structures, thanks to studies of new bacterial species, improvements in sample preparation that avoid the addition of artifacts, and gains in resolution. This is the case of the recently described structures "nanopods" and "hami" (Shetty et al., 2011; Moissl et al., 2005).

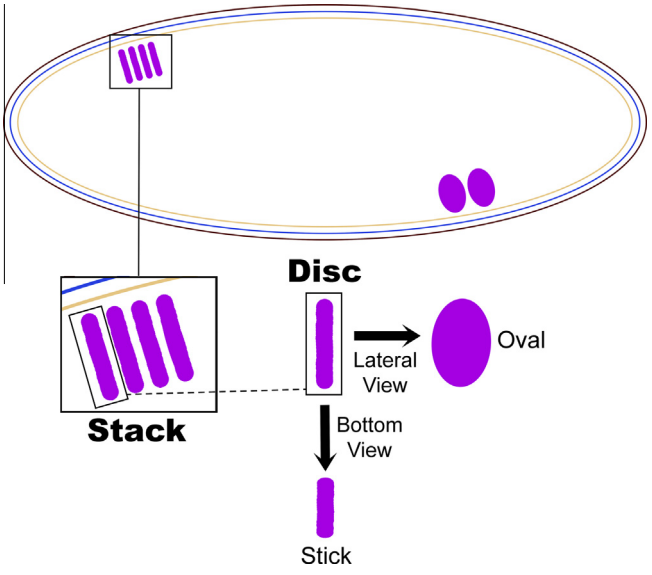

Fig.1. Model of a *P. deceptionensis* M1^T cell showing Stacks in the cytoplasm. A pile of four subunits integrates the Stack in the squared area. The lateral and bottom view of the squared subunit are shown. In 2D, the Stack can be observed as an oval structure or as a pile of sticks. Pink: Stacks; red: outer membrane; blue: peptidoglycan layer; cream-color: PM. (For interpretation of the references to color in this figure legend, the reader is referred to the web version of this article.)

In our previous work, we described a new bacterial structure termed a "Stack", which was revealed by different electron microscopy techniques and electron tomography and CEMOVIS (Delgado et al., 2013). Stacks, which were observed in bacteria of the *Pseudomonas* genus, were defined as piles of oval disc subunits surrounded by a membrane-like structure and localized in the cell cytoplasm. Stacks can be present in variable number within each cell, separately or grouped together, frequently very close to the plasma membrane (PM). In three-dimensional views (3D), each subunit appears as a flat oval disc, while in two-dimensional views (2D) the Stack is seen either as an oval structure or a pile of sticks (Fig. 1). The function of Stacks was not elucidated, but they were mostly observed very close to DNA fibers, suggesting they could be somehow related to the bacterial chromosome dynamics and/or the cell replication process.

Our goal in the current work was to refine the structural characterization of Stacks using methods known to preserve bacterial cell structures very close to their native state, and to rule out their possible origin as artifacts derived from the sample preparation methods. We imaged the architecture of Stacks within the whole bacterial cell by CET of plunge-frozen whole bacteria. We also applied cryo-electron tomography of vitreous sections (CETOVIS) to high-pressure frozen bacteria in an attempt to achieve molecular details not provided by previously used techniques.

2. Materials and methods

2.1. Cell growth

Studies were performed in *Pseudomonas deceptionensis* M1^T (LMG 25555) isolated from marine sediments collected in Deception Island (Antarctica) and characterized by our group as a new species (Carrión et al., 2011). *P. deceptionensis* M1^T was grown for 12 days at 0°C on tryptone soy agar (TSA, Oxoid) according to the manufacturer's specifications, unless otherwise specified.

2.2. Plunge freezing

Colonies of bacteria were suspended in milliQ water, centrifuged at 3000 rpm for 8 min and the supernatant was discarded. The process was repeated twice. Then, bacteria cells were resuspended in milliQ water. One drop of the suspension was applied on the carbon surface of a glow-discharged Quantifoil®200 mesh copper grid (Quantifoil Micro Tools, Jena, Germany). The sample was maintained at 100% humidity and the excess of liquid was blotted with filter paper, a thin film of suspension remaining on the grid. The sample was cryo-immobilized by plunging the grid into liquefied ethane using the Vitrobot Mark III (FEI Company, Eindhoven, Netherlands). The vitrified samples were stored in liquid nitrogen (LN_2) until their observation in the cryo-electron microscope.

2.3. High-pressure freezing (HPF)

HPF of samples was performed on colonies resuspended in 30% dextran (Fluka) in 0.01 M phosphate buffer saline (PBS) (Delgado et al., 2013). The suspensions were introduced into 350 μm inner diameter copper tubes and ultrarapidly frozen using a Leica EMPACT High-Pressure Freezer (Leica Microsystems, Vienna, Austria). The copper tubes were stored in LN_2 until further use for cryo-sectioning.

2.4. Vitreous cryo-sectioning

Quantifoil® carbon-coated 200 mesh copper grids were used to pick up the vitreous sections (VIS). Firstly, fiducial markers were

attached to the carbon of the grids by successively floating them on drops of protein A coupled to 10-nm diameter colloidal gold particles (CMC, University of Utrecht, The Netherlands) 1:500 in 0.01 M PBS and distilled water (Delgado et al., 2013). The grids were left in a dry chamber for at least 2 h before being used.

Secondly, copper tubes from the HPF and stored in LN_2 were transferred to a pre-cooled (−150°C) FC6 cryo-ultramicrotome (Leica Microsystems, Vienna, Austria) covered with a homemade anticontamination glove box (Pierson et al., 2010). An influx of dry nitrogen gas, dry sodium hydroxide pellets and dry silica gel balls were used to reduce the relative humidity within the chamber to values close to 0%. Squared block faces with side measures between 80 and 100 μm were trimmed from the copper tubes in black uniform areas of the sample, using a 45° cryo-trim diamond blade (Diatome, Biel, Switzerland). The grids containing the fiducial markers were then glow-discharged to facilitate the attachment of the ribbons.

VIS of 50 nm were cut with a 35° diamond knife (Diatome, Biel, Switzerland) with a clearance angle of 6° and cutting speeds between 0.3 and 100 mm/s. The ribbons were attached to the grids by successively applying electrostatic charge (Pierson et al., 2010) and the stamping method. The electrostatic charging was performed with the CRION (Leica Microsystems, Vienna, Austria) and the stamping method with the section flattening position of the cryotool base plate (Leica Microsystems, Vienna, Austria). The grids supporting the attached VIS were transferred to grid boxes and stored in LN_2 until observed.

2.5. TEM imaging

VIS of samples and plunge-frozen samples were transferred to a Tecnai F20 EM (FEI, Eindhoven, The Netherlands) using a cryo-holder (Gatan, Pleasanton, USA). The samples were examined at 200 kV, at a temperature ranging from −175 to −170°C and using low-dose imaging conditions. Electron diffraction was used to check whether the water was vitreous or crystalline; crystalline samples were discarded. Low-dose images and tilt series, with exposures between 0.8 and 1 electron per $Å^2$ and under-focus values of 6 nm, were recorded with a 4096 × 4096 pixel CCD Eagle camera (FEI, Eindhoven, The Netherlands) at ×29000 and ×25000, for VIS and for plunge-frozen specimens, respectively. For tomography, the tilt series were collected using the Xplore3D (FEI, Eindhoven, The Netherlands) acquisition program. The angular tilt range was typically set from −60° to +60° with a 1.5–2°-tilt increase.

3. 3D reconstructions and post-processing

The tilt series were aligned through 10-nm gold fiducial markers using the IMOD 4.5.3 software (Kremer et al., 1996). The aligned series were then processed by the simultaneous iterative reconstruction technique (SIRT) in the Tomo3D package, version of April 2012 (Agulleiro and Fernández, 2011; Agulleiro et al., 2010). Tomograms were denoised using edge-enhancing anisotropic non-linear diffusion filtering through the TomoEED program, TOMOAND package, version of September 2011 (Fernández et al., 2007; Fernández and Sam, 2005; Fernández and Li, 2003). Finally, tomograms were analyzed using IMOD (xyz slicer).

3.1. Measurements and statistical analysis

To analyze width differences between the PM and the membrane surrounding the Stack subunits, as well as the length and width of each subunit and the distance between them, 23 bacteria were observed and at least 40 measurements of each parameter were done. The one-factor ANOVA test was used. Significance was set at $p < 0.05$. The analyses were carried out using Statgraphics software (version 5.1).

3.2. Confocal microscopy preparation

Dubellco's PBS was added to a TSA plate containing isolated colonies of *P. deceptionensis* $M1^T$. Cells were then scrapped and the suspension was saved in an Eppendorf. The sample was twice centrifuged at 10,000 rpm for 2.5 min, the supernatant was removed and the pellet resuspended in Dubellco's PBS in order to eliminate the excess of mucus produced by this strain, which may affect the fluorescent labeling of membranes. The FM4-64 reactive (Molecular Probes) was added at a final concentration of 5 μg/ml and the suspension was kept in agitation and darkness for 1 h. The labeled sample was centrifuged at 10,000 rpm for 2.5 min, the supernatant was discarded and the pellet resuspended in Dubellco's PBS. On a microscope slide, the suspension was mixed 1:1 (v/v) with 0.7% low-melting agarose. Images were acquired with a TCS-SP2 Leica confocal microscope using a 63× oil immersion objective (excitation wavelength 515 nm, and emission wavelength 640 nm).

4. Results and discussion

In a previous article (Delgado et al., 2013), we described for the first time a bacterial cytoplasmic structure referred to as a "Stack". We used a variety of electron microscopy techniques to decipher this unusual structural feature, including TEM observation of high-pressure frozen and freeze-substituted (HPF-FS), Tokuyasu and freeze-fractured samples. We also made a first attempt to visualize Stacks in their native state by CEMOVIS. The combination of these techniques provided us with different complementary images of the Stacks, which suggested that the new structure was not a methodological artifact.

In the present study, we visualized the Stacks in the context of the whole cell by Cryo-EM, as this technique is less artifactual and would provide views of the new structure in a near-native state (Chang et al., 2014; Hoenger, 2014; Comolli et al., 2013; Milne et al., 2013), thus increasing our knowledge of its architecture and organization. Cryo-EM was therefore employed to image plunge-frozen whole cells of the Antarctic bacterium *P. deceptionensis* $M1^T$, between 1.5 and 2 μm long and with a diameter of 0.8 μm. Stacks were again revealed in the peripheral regions of the bacteria, verifying that they were not artifacts derived from previously used preparation methods (Figs. 2A–D and 3A–D). They were only visible in areas thin enough to allow an electron beam to pass through, which corresponded to the peripheral areas of the cell. Measurements of the length and width of the Stack subunits in images with a pixel size of 0.81 nm provided the mean values 90.7 ± 25 nm and 13.3 ± 1.7 nm, respectively. In the context of the whole cell, it was confirmed that the discs varied in length, whereas the width was practically constant, as we had previously observed in sections of bacterial samples prepared with other techniques.

To refine the 3D views of Stacks reconstructed from Epon sections (Delgado et al., 2013), we recorded a new tomographic tilt series by Cryo-EM. CET of the interior architecture of intact bacteria is a powerful technique for unraveling internal bacterial structures (Chang et al., 2014; Hoenger, 2014; Comolli et al., 2013; Milne et al., 2013). Nevertheless, the Stacks were not easily identified, because they did not possess a strong intrinsic contrast, unlike what occurs with magnetosomes (Scheffel et al., 2006) or some storage granules (Iancu et al., 2010). Slices showed the Stacks

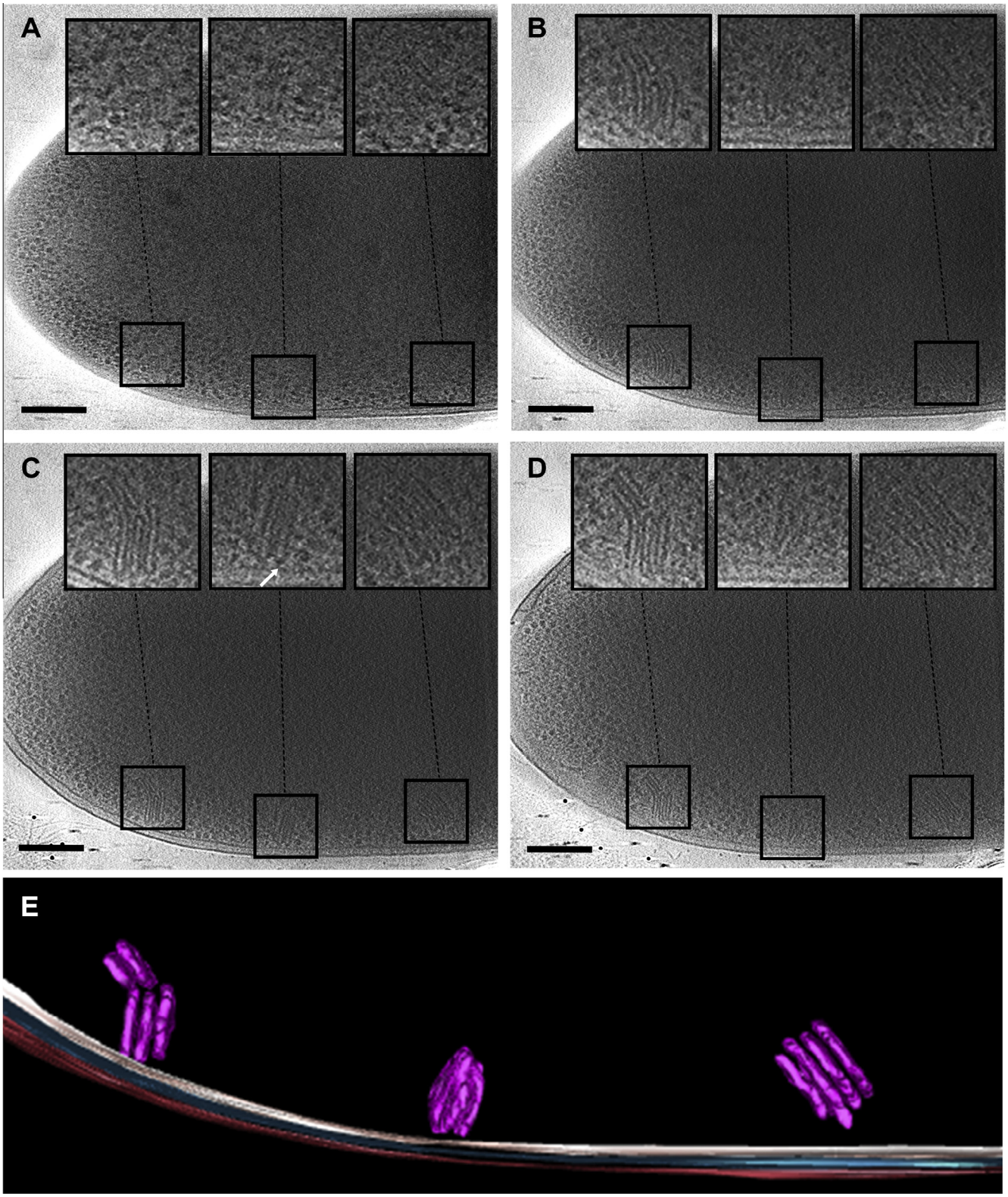

Fig.2. Stacks analyzed by CET of plunge-frozen whole bacteria. (A–D) 2-nm slices of a tomogram reconstructed from a plunge-frozen *P. deceptionensis* M1^T cell. (E) Partial segmentation of the tomogram observed in (A–D). Pink: Stacks; red: outer membrane; blue: peptidoglycan layer; cream-color: PM. Four Stacks are observed in three different peripheral locations inside the cytoplasm, at variable angles with respect to the PM. The two on the left are in the same location, but they differ in their respective orientations. The other two appear isolated in their respective locations (A–E). Objective lens defocus: −6 μm. Pixel size: 0.85 nm. Scale bars = 200 nm. (For interpretation of the references to color in this figure legend, the reader is referred to the web version of this article.)

located near the inside perimeter of the *P. deceptionensis* M1^T cells and oriented at angles of 35–90° to the PM. They appeared isolated within the cell cytoplasm or in groups of variable orientation (Figs. 2 and 3). The 3D distribution described from bacterial Epon sections in our previous work was therefore confirmed in the whole bacterial cell.

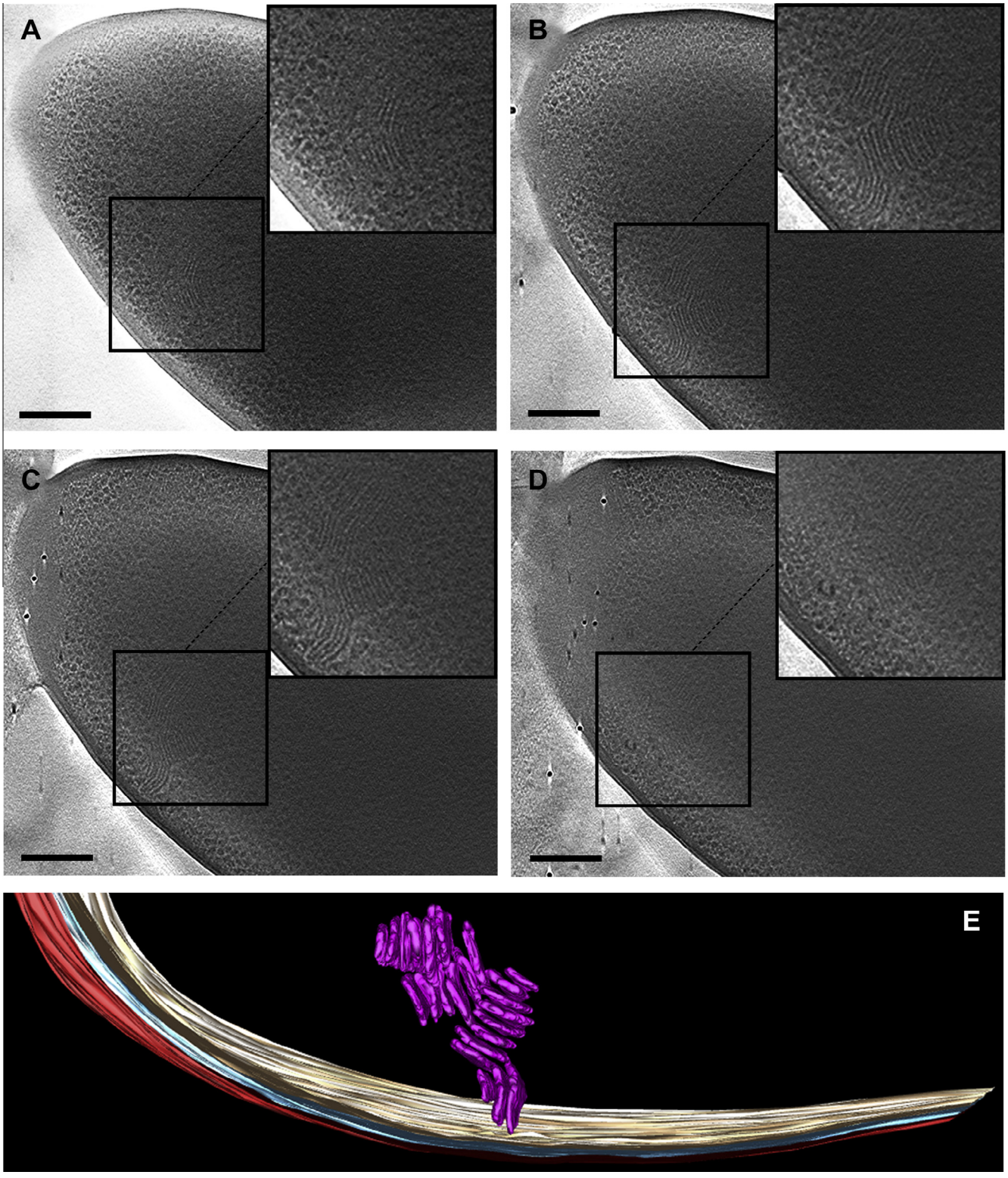

Fig.3. Stacks analyzed by CET of plunge-frozen whole bacteria. (A–D) 2-nm slices of a tomogram reconstructed from a plunge-frozen *P. deceptionensis* M1^T cell. (E) Partial segmentation of the tomogram observed in (A–D). Pink: Stacks; red: outer membrane; blue: peptidoglycan layer; cream-color: PM. Four grouped Stacks are clearly observed in the same peripheral location inside the cytoplasm. Objective lens defocus: −6 μm. Pixel size: 0.85 nm. Scale bars = 200 nm. (For interpretation of the references to color in this figure legend, the reader is referred to the web version of this article.)

The appearance of Stacks in the tomogram slices bore a resemblance to the structure of the type 6 secretion system (T6SS). T6SS forms highly dynamic intracellular tubes, which assemble and disassemble in a few seconds at different subcellular locations (Chang et al., 2014; Basler et al., 2012). Moreover, both structures, Stacks and T6SS, are oriented roughly perpendicular to the PM and are located exclusively in the cytosol. However, T6SS systems are clearly different in their longer length and narrower width in their "extended" conformation, as well as in having a straight and tubular structure and being connected to the cell membrane by a

distinct basal structure. In contrast, after tomogram analysis, Stacks were visualized as a pile of oval discs, surrounded by a membrane, located close to but not attached to the PM, strongly indicating they were a completely different structure.

Several Stacks were visualized forming a group, as shown in Fig. 3, with one Stack very close to the PM, while the others, contiguous and variably oriented, extended towards the most internal and thickest part of the bacteria. However, the segmentation could not cover more than four Stacks. Electron tomography requires specimens to be sufficiently thin for the electron beam to be transmitted, typically not much more than ~0.5 μ, even for microscopes able to operate at 200–300 kV (Milne et al., 2013; Gan and Jensen, 2012; Koster et al., 1997). *P. deceptionensis* M1^T cells, with a length of 1.5–2 μm and a diameter of 0.8 μm, surpass this limit and thus the partial field of view of the plunge-frozen whole cells did not allow us to determine the exact number of Stacks forming a group (Fig. 3A–D). Figs. 2E and 3E illustrate the peripheral segmentation of Stacks observed in the tomogram slices in Figs. 2A–D and 3A–D, respectively.

In the plunge-frozen bacteria, it was seen that each subunit forming a Stack was clearly delimited by an electron-dense layer resembling a lipid membrane. In plunge-frozen cells the bilayer aspect of the PM is not usually resolved (Hoffmann et al., 2008), therefore it was not possible to see if the membrane surrounding the Stacked discs matched the PM. Thus, to compare the two membranes, we measured the widths of the layer surrounding the discs and the PM, obtaining mean values of 4.2 ± 0.8 nm and 6 ± 1.1 nm, respectively. When measurements obtained from plunge-frozen whole bacteria were analyzed by the one-factor ANOVA test, the p-value < 0.0001 revealed significant differences between the widths of both membrane types, suggesting a different composition. The mean value obtained for the width of the PM of *P. deceptionensis* M1^T, 6 ± 1.1 nm, matched the values obtained with this technique in other bacteria, for example, around 7 nm for mycobacteria (Hoffmann et al., 2008). Zuber and co-workers (2008) also reported the dimensions of cell envelope structures, including PM, of different mycobacteria, corynebacteria and *Escherichia coli* cells, although based on CEMOVIS analysis. The mean values obtained for the PM of these bacterial species ranged from 5.5 to 7.1 nm, which are similar to the width value found for the PM of *P. deceptionensis* M1^T in the context of the whole cell. Notably, the values of the PM width of the different bacteria were always significantly higher than those of the Stack disc membrane.

It is noteworthy that the mean PM width obtained from the plunge-frozen *P. deceptionensis* M1^{T}cells was slightly higher than when measuring the same structure in VIS in our previous work (Delgado et al., 2013). This difference can be understood considering that vitreous cryo-section-induced compression influences the interpretation and reliability of electron microscopy images. The artifacts inherent to VIS (mainly compression and crevasses) differentially deform the sample depending on its orientation with regard to the cutting direction (Al-Amoudi et al., 2005; Richter, 1994; Chang et al., 1983; McDowall et al., 1983).

As reported by Pierson and co-workers (2011), VIS-induced compression is non-uniform among sectioned whole cells and their intracellular macromolecular complexes. These authors demonstrated that some cellular nanomachines, such as ribosomes, are not affected by compression and therefore VIS and CETOVIS are suitable techniques for charting the structural organization of intracellular and isolated ribosomes (Pierson et al., 2011). In contrast, as Stacks are a larger macromolecular assembly of membrane-enclosed discs, the possibility that they are affected by VIS-induced compression is reasonably higher. Therefore, the plunge-freezing technique allowed Stacks to be visualized without the typical artifacts associated with mechanical cutting, which can affect the shape and, consequently, the dimension of cells and large structures.

Another interesting feature observed throughout the tomograms was the absence of continuity between the membrane surrounding the Stack subunits and the PM. This fact suggests that Stacks are not invaginations of the PM, which occur in, for example, photosynthetic and nitrifying bacteria (Niederman, 2006). Whole-mount cryo-electron tomography was used by Konorty et al. (2008) to analyze the intracellular architecture of the anaerobic purple photosynthetic *Rhodopseudomonas viridis*. Tomogram slices showed membranes in a lamellar arrangement with a certain similarity to Stack disc assemblies, except that the photosynthetic membranes are clearly connected to the cell membrane by small tunnel-like structures that form a continuum with the periplasmic compartment. This point, together with the Stack length and architecture and their almost parallel distribution to the PM, all clearly differentiate these novel structures from bacterial cell membrane invaginations (Konorty et al., 2008).

Nevertheless, because of the limitations of the techniques used, the possibility that Stacks are extensions of the PM cannot be definitively discarded. Samples of bacterial or mammalian cells

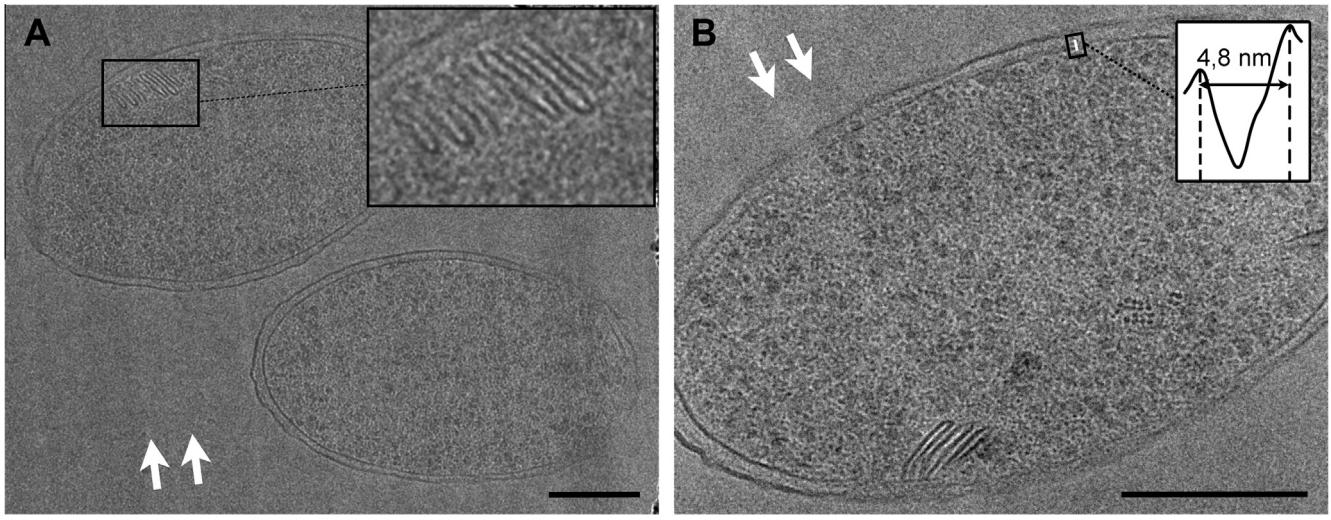

Fig.4. CEMOVIS of Stacks in *P. deceptionensis* M1^T. (A and B) 50-nm VIS. Stacks are observed in the peripheral cytoplasm of *P. deceptionensis* M1^{T}cells, close to the PM and oriented at different angles with respect to the PM. (B) A density profile of a section of the PM is observed in the squared area, revealing the lipid bilayer pattern. White arrows indicate the cutting directions. Scale bars = 200 nm.

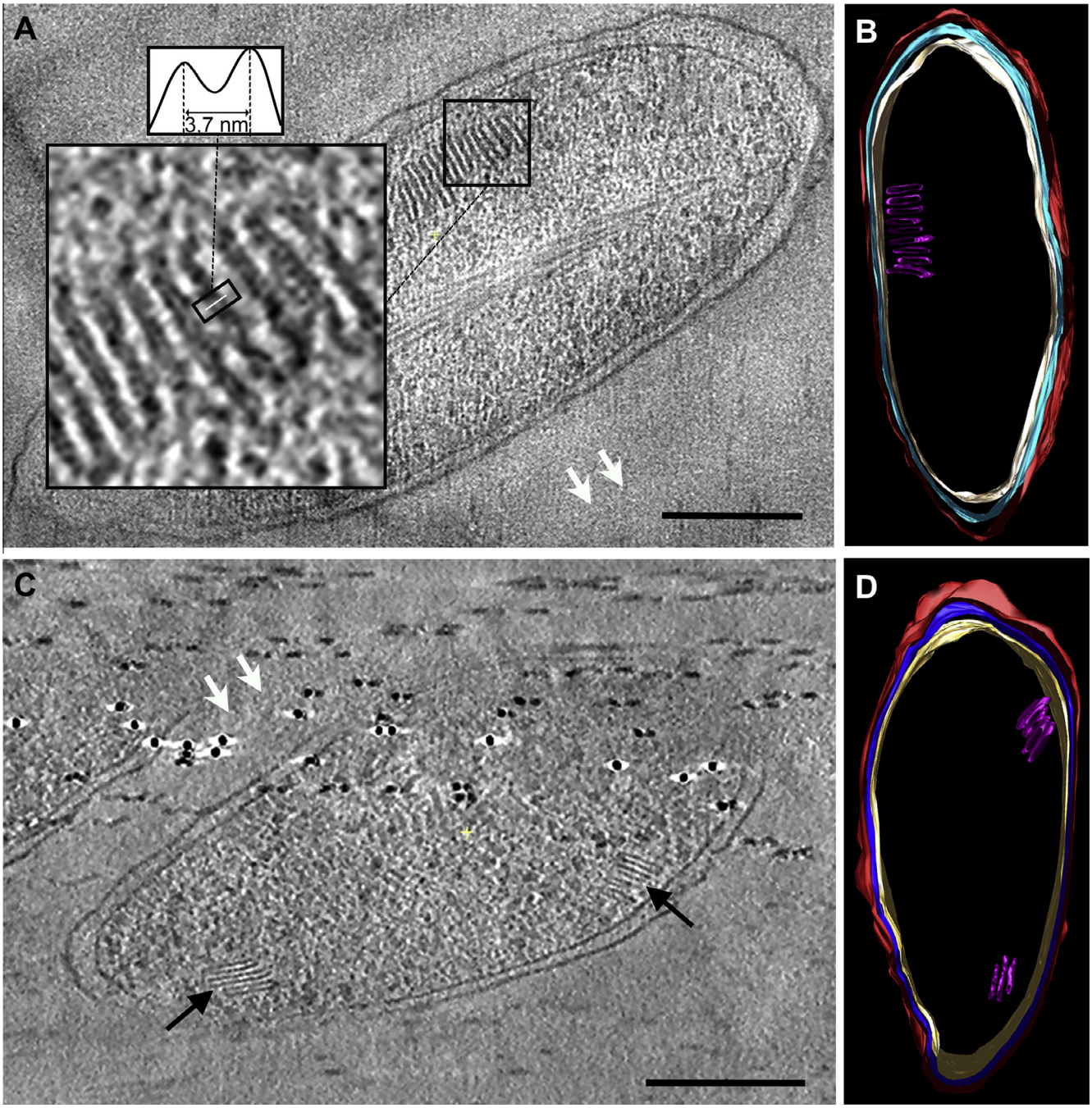

Fig.5. Stacks analyzed by CETOVIS. (A and C) 1-nm slices of tomograms reconstructed from 50-nm VIS of *P. deceptionensis* M1^T. Objective lens defocus: −6 μm. Pixel size: 0.71 nm. (A) The magnified square shows a fragment of a Stack whose subunits are surrounded by a membrane-like structure exhibiting the typical pattern of a lipid bilayer membrane. The density profile of a section of the membrane-like structure surrounding the discs is observed in the upper squared area, revealing the two peaks typical of a lipid bilayer membrane. (C) Two isolated Stacks are observed in different positions within the cytoplasm of the bacterial cell. (B and D) Segmentations of the tomograms observed in (A) and (C), respectively. Pink: Stacks; red: outer membrane; blue: peptidoglycan layer; cream-color: PM. White arrows indicate the cutting direction. Scale bars = 200 nm. (For interpretation of the references to color in this figure legend, the reader is referred to the web version of this article.)

can be thinned under cryogenic conditions using cryo-focused-ion-beam milling (cryo-FIB) (Villa et al., 2013; Rigort et al., 2010; Marko et al., 2006). Cryo-FIB provides sections between 100 and 300 nm, with wider fields of view than VIS and at good resolution, so therefore this technique could provide fresh insight into this issue in future studies.

Our approach did reveal possible points of physical contact between some Stack subunits and the cell membrane (Fig. 2C, see arrow), which might correspond to a kind of molecular anchorage that retains Stacks at the peripheral areas of the cytoplasm. In any case, these hypothetical physical connections take up about 1–2 pixels, which coincides with the size of the noise, so further experiments are required to verify their existence.

To shed more light on the nature of the membrane that surrounds the Stacked discs, we analyzed 50-nm VIS of high-pressure frozen *P. deceptionensis* M1^T cells by TEM, which provided a better resolution than the plunge-frozen whole specimens (Fig. 4A and B). Depending on the orientation of the VIS with respect to the cells, the lipid bilayer pattern of the PM was observed, with the typical two-peak density profile (Fig. 4B, see

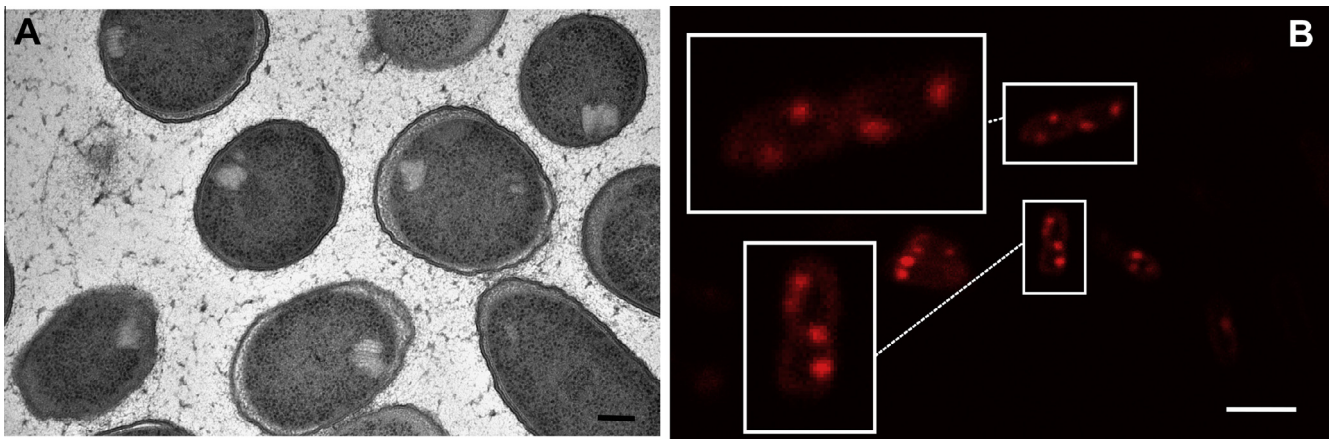

Fig.6. Stacks analyzed by confocal microscopy. (A) TEM view of an Epon section of *P. deceptionensis* M1^T cells processed by HPF-FS. Stacks are viewed at the peripheral region of the cells and at different locations inside. Scale bar = 200 nm. (B) FM4-64 fluorescent labeling of *P. deceptionensis* M1^T cells. Bacteria show fluorescent contours, corresponding to the cell PM, and peripheral fluorescent dots in the cytoplasm. Scale bar = 5 μm.

squared area). The layer delimiting each Stack subunit presented similar electron-density to the PM, but no bilayer pattern was discernible (Fig. 4A and B). CETOVIS was then carried out, recording tilt series of images from −60° to +60°, and the subsequent 4-nm resolution tomograms revealed that through the *z*-axis the Stacks were composed of discs clearly delimited by membrane-like structures (Fig. 5A and C). Additionally, analysis of tomograms obtained from VIS revealed a lipid bilayer membrane pattern in the layer surrounding each disc (Fig. 5A, see magnified area), which was confirmed by the density profile (Fig. 5A). It is notable that when Stacks were observed in VIS tomograms, the lipid bilayer of the PM was frequently not resolved. As Stacks are localized in the peripheral regions of the bacterial cytoplasm, the section cutting may occur away from the central plane, so that the membrane is not cut perpendicularly and the gap of the bilayer structure is obliterated by the overlapping head group regions, thus obscuring the membrane bilayer pattern. Since the Stacks appeared clearly delimited throughout the *z*-axis, more reliable segmentations of the structures were carried out (Fig. 5B and D).

Another possible way of obtaining new information about the lipid nature of the bilayer membrane surrounding each Stack subunit was to use confocal fluorescence microscopy to image *P. deceptionensis* M1^T cells labeled with FM4-64 reagent, which specifically binds to membrane lipid bilayers (Wikström et al., 2009). Fluorescent labeling was observed not only on the cell PM, but also as dots inside the cytoplasm (Fig. 6B). The latter were detected mostly in the peripheral region of cells, which matched the location of the Stacks (Fig. 6A). Taking into account that previous observations of *P. deceptionensis* M1^T cells by TEM and Cryo-EM in the assayed conditions did not show any kind of intracytoplasmic membranous structures other than Stacks (Delgado et al., 2013), the confocal microscopy supported the lipid nature of the Stack disc membrane. Further experiments, such as correlative light and electron microscopy (CLEM), would be required for more definitive proof.

It should be noted that the Stacked discs forming the novel structures were separated by an apparently constant distance. Measures of the distance between these subunits were taken from plunge-frozen cells, obtaining a mean value of 5.2 ± 1.3 nm. However, analysis of the *X*, *Y* and *Z* planes of the tomograms from CET of plunge-frozen whole bacteria and CETOVIS did not reveal any consistent repetitive structural characteristics among the subunits, so we were unable to apply subtomogram averaging to decipher possible linking features.

Equally as important as discerning the structural details of Stacks is to find their functional role. In our previous study, Stacks were mostly observed very close to DNA fibers, suggesting they could be somehow related to bacterial chromosome dynamics. However, as we are dealing with a new bacterium, a major problem in defining Stack function is that no tools are currently available to localize the proteins potentially involved in processes such as chromosome replication or segregation. Another difficulty is that, after many attempts, we have been unable to observe Stacks in cells growing in liquid cultures. It was consequently impossible to obtain synchronized cultures to definitively associate Stacks with a particular growth phase. These cytoplasmic structures were only visualized at a frequency suitable for their study when *P. deceptionensis* M1^T cells grew in solid media at 0°C and 12 days of incubation, parameters that were therefore fixed throughout our structural studies.

In the present study, in an attempt to relate Stacks with the replication process, *P. deceptionensis* M1^T cells were grown in TSA at 0°C for different incubation periods (6, 12 and 20 days) and processed by HPF-FS according to a previously described technique (Delgado et al., 2013). The number of dividing cells and Stacks were quantified, counting as dividing cells those that presented a recognizable septum of division (Table 1). Although we are aware that these results are not conclusive, it was notable that the number of cells containing Stacks changed with the incubation time and the percentage of dividing cells. After 6 days of incubation, no Stacks were detected, although dividing cells were present. The next sample, at 12 days of incubation, showed a slight decrease in the percentage of dividing cells but a great increase in the number of Stack-containing cells. Finally, after 20 days of incubation, when dividing cells were almost undetectable, the number of Stacks dropped drastically. With a great deal of caution, we could say that the presence of Stacks is somehow related with a certain phase of the division process. In order to avoid any bias associated

Table 1
Percentages of bacterial cells containing Stacks in their cytoplasm and dividing bacterial cells (with division septum) from Epon sections of *P. deceptionensis* M1^T cells grown on TSA at 0°C and processed by HPF-FS.

Incubation Time (days)	N Bacteria	% Bacteria with Stacks	% Dividing Bacteria
6	283	0	8.83
12	452	23.67	6.86
20	471	2.55	0.21

with the sampling process, several colonies of bacteria were mixed just before taking the sample to be cryo-immobilized. Moreover, as we were evaluating 60-nm sections of the bacteria, the number of bacteria analyzed in each case was sufficiently large to discard sampling-related deviations.

The combination of CET of plunge-frozen whole bacteria and CETOVIS has proved useful in providing reliable structural information about these new bacterial cytoplasmic structures at different resolution levels and in a general cellular context. The complementary information obtained with both techniques enabled us to definitively discard the possible artifactual nature of the Stacks, which undoubtedly deserve further study both at structural and functional levels.

Acknowledgments

We thank José Jesús Fernández (CNB) for his help in tomography. This study was supported by the Government of Spain (CICYT project CTQ 2010-21183-C02-01/PPQ) and by the Autonomous Government of Catalonia (Grant 2009SGR1212).

Appendix A. Supplementary data

Supplementary data associated with this article can be found, in the online version, at http://dx.doi.org/10.1016/j.jsb.2015.01.008.

References

Agulleiro, J.I., Fernández, J.J., 2011. Fast tomographic reconstruction on multicore computers. Bioinformatics 27, 582–583. http://dx.doi.org/10.1093/bioinformatics/btq692.

Agulleiro, J.I., Garzón, E.M., García, I., Fernández, J.J., 2010. Vectorization with SIMD extensions speeds up reconstruction in electron tomography. J. Struct. Biol. 170, 570–575. http://dx.doi.org/10.1016/j.jsb.2010.01.008.

Al-Amoudi, A., Chang, J.J., Leforestier, A., McDowall, A., Salamin, L.M., Norlen, L.P.O., Richter, K., Blanc, N.S., Studer, D., Dubochet, J., 2004. Cryo-electron microscopy of vitreous sections. EMBO J. 23, 3583–3588. http://dx.doi.org/10.1038/sj.emboj.7600366.

Al-Amoudi, A., Studer, D., Dubochet, J., 2005. Cutting artefacts and cutting process in vitreous sections for cryo-electron microscopy. J. Struct. Biol. 150, 109–121. http://dx.doi.org/10.1016/j.jsb.2005.01.003.

Basler, M., Pilhofer, M., Henderson, G.P., Jensen, G.J., Mekalanos, J.J., 2012. Type VI secretion requires a dynamic contractile phage tail-like structure. Nature 483, 182–186. http://dx.doi.org/10.1038/nature10846.

Beeby, M., Cho, M., Stubbe, J., Jensen, G.J., 2012. Growth and localization of polyhydroxybutyrate granules in *Ralstonia eutropha*. J. Bacteriol. 194, 1092–1099. http://dx.doi.org/10.1128/JB.06125-11.

Briegel, A., Dias, D.P., Li, Z., Jensen, R.B., Frangakis, A.S., Jensen, G.J., 2006. Multiple large filament bundles observed in *Caulobacter crescentus* by electron cryotomography. Mol. Microbiol. 62, 5–14. http://dx.doi.org/10.1111/j.1365-2958.2006.05355.x.

Briegel, A., Ding, H.J., Li, Z., Werner, J., Gitai, Z., Dias, D.P., Jensen, R.B., Jensen, G.J., 2008. Location and architecture of the Caulobacter crescentus chemoreceptor array. Mol. Microbiol. 69, 30–41. http://dx.doi.org/10.1111/j.1365-2958.2008.06219.x.

Carrión, O., Miñana-Galbis, D., Montes, M.J., Mercadé, E., 2011. *Pseudomonas deceptionensis* sp. nov., a psychrotolerant bacterium from the Antarctic. Int. J. Syst. Evol. Microbiol. 61, 2401–2405. http://dx.doi.org/10.1099/ijs.0.024919-0.

Chang, J.J., McDowall, A.W., Lepault, J., Freeman, R., Walter, C.A., Dubochet, J., 1983. Freezing, sectioning and observation artefacts of frozen hydrated sections for electron microscopy. J. Microsc. 132, 109–123. http://dx.doi.org/10.1111/j.1365-2818.1983.tb04714.x.

Chang, Y.W., Chen, S., Tocheva, E.I., Treuner-Lange, A., Löbach, S., Søgaard-Andersen, L., Jensen, G.J., 2014. Correlated cryogenic photoactivated localization microscopy and cryo-electron tomography. Nat. Methods 11, 737–739. http://dx.doi.org/10.1038/nmeth.2961.

Chen, S., Beeby, M., Murphy, G.E., Leadbetter, J.R., Hendrixson, D.R., Briegel, A., Li, Z., Shi, J., Tocheva, E.I., Müller, A., Dobro, M.J., Jensen, G.J., 2011. Structural diversity of bacterial flagellar motors. EMBO J. 30, 2972–2981. http://dx.doi.org/10.1038/emboj.2011.186.

Chen, S., McDowall, A., Dobro, M.J., Briegel, A., Ladinsky, M., Shi, J., Tocheva, E.I., Beeby, M., Pilhofer, M., Ding, H.J., Li, Z., Gan, L., Morris, D.M., Jensen, G.J., 2010. Electron cryotomography of bacterial cells. J. Vis. Exp., doi:103791/1943.

Comolli, L.R., Baker, B.J., Downing, K.H., Siegerist, C.E., Banfield, J.F., 2008. Three-dimensional analysis of the structure and ecology of a novel, ultra-small archaeon. ISME J. 3, 159–167. http://dx.doi.org/10.1038/ismej.2008.99.

Comolli, L.R., Kundmann, M., Downing, K.H., 2006. Characterization of intact subcellular bodies in whole bacteria by cryo-electron tomography and spectroscopic imaging. J. Microsc. 223, 40–52. http://dx.doi.org/10.1111/j.1365-2818.2006.01597.x.

Comolli, L.R., Luef, B., Chan, C.S., 2011. High-resolution 2D and 3D cryo-TEM reveals structural adaptations of two stalk-forming bacteria to an Fe-oxidizing lifestyle. Environ. Microbiol. 13, 2915–2929. http://dx.doi.org/10.1111/j.1462-2920.2011.02567.x.

Comolli, L.R., Siegerist, C.E., Shin, S.H., Bertozzi, C., Regan, W., Zettl, A., De Yoreo, J., 2013. Conformational transitions at an S-layer growing boundary resolved by cryo-TEM. Angew. Chem. Int. Ed. Engl. 52, 4829–4832. http://dx.doi.org/10.1002/anie.201300543.

Delgado, L., Carrión, O., Martínez, G., López-Iglesias, C., Mercadé, E., 2013. The Stack: a new bacterial structure analyzed in the Antarctic bacterium *Pseudomonas deceptionensis* M1^T by transmission electron microscopy and tomography. PLoS ONE 8, e73297. http://dx.doi.org/10.1371/journal.pone.0073297.

Erickson, H.P., 1997. FtsZ, a tubulin homologue in prokaryote cell division. Trends Cell Biol. 7, 362–367. http://dx.doi.org/10.1016/S0962-8924(97)01108-2.

Fernández, J.J., Li, S., 2003. An improved algorithm for anisotropic nonlinear diffusion for denoising cryo-tomograms. J. Struct. Biol. 144, 152–161. http://dx.doi.org/10.1016/j.jsb.2003.09.010.

Fernández, J.J., Li, S., Lucic, V., 2007. Three-dimensional anisotropic noise reduction with automated parameter tuning: application to electron cryotomography. In: Borrajo, D., Castillo, L., Corchado, J.M. (Eds.), Current Topics in Artificial Intelligence, Lecture Notes in Computer Science. Springer, Heidelberg, Berlin, pp. 60–69.

Fernández, J.J., Sam, L., 2005. Anisotropic nonlinear filtering of cellular structures in cryoelectron tomography. Comput. Sci. Eng. 7, 54–61. http://dx.doi.org/10.1109/MCSE.2005.89.

Gan, L., Jensen, G.J., 2012. Electron tomography of cells. Q. Rev. Biophys. 45, 27–56. http://dx.doi.org/10.1017/S0033583511000102.

Hoenger, A., 2014. High-resolution cryo-electron microscopy on macromolecular complexes and cell organelles. Protoplasma. http://dx.doi.org/10.1007/s00709-013-0600-1.

Hoenger, A., McIntosh, J.R., 2009. Probing the macromolecular organization of cells by electron tomography. Curr. Opin. Cell Biol. 21, 89–96. http://dx.doi.org/10.1016/j.ceb.2008.12.003.

Hoffmann, C., Leis, A., Niederweis, M., Plitzko, J.M., Engelhardt, H., 2008. Disclosure of the mycobacterial outer membrane: Cryo-electron tomography and vitreous sections reveal the lipid bilayer structure. Proc. Natl. Acad. Sci. 105, 3963–3967. http://dx.doi.org/10.1073/pnas.0709530105.

Iancu, C.V., Morris, D.M., Dou, Z., Heinhorst, S., Cannon, G.C., Jensen, G.J., 2010. Organization, structure, and assembly of α-carboxysomes determined by electron cryotomography of intact cells. J. Mol. Biol. 396, 105–117. http://dx.doi.org/10.1016/j.jmb.2009.11.019.

Ingerson-Mahar, M., Briegel, A., Werner, J.N., Jensen, G.J., Gitai, Z., 2010. The metabolic enzyme CTP synthase forms cytoskeletal filaments. Nat. Cell Biol. 12, 739–746. http://dx.doi.org/10.1038/ncb2087.

Jensen, G.J., Briegel, A., 2007. How electron cryotomography is opening a new window onto prokaryotic ultrastructure. Curr. Opin. Struct. Biol. 17, 260–267. http://dx.doi.org/10.1016/j.sbi.2007.03.002.

Khursigara, C.M., Wu, X., Subramaniam, S., 2008. Chemoreceptors in *Caulobacter crescentus*: trimers of receptor dimers in a partially ordered hexagonally packed array. J. Bacteriol. 190, 6805–6810. http://dx.doi.org/10.1128/JB.00640-08.

Kishimoto-Okada, A., Murakami, S., Ito, Y., Horii, N., Furukawa, H., Takagi, J., Iwasaki, K., 2010. Comparison of the envelope architecture of *E. coli* using two methods: CEMOVIS and cryo-electron tomography. J. Electron. Microsc. (Tokyo) 59, 419–426. http://dx.doi.org/10.1093/jmicro/dfq056.

Komeili, A., Li, Z., Newman, D.K., Jensen, G.J., 2006. Magnetosomes are cell membrane invaginations organized by the actin-like protein MamK. Science 311, 242–245. http://dx.doi.org/10.1126/science.1123231.

Konorty, M., Kahana, N., Linaroudis, A., Minsky, A., Medalia, O., 2008. Structural analysis of photosynthetic membranes by cryo-electron tomography of intact *Rhodopseudomonas viridis* cells. J. Struct. Biol. 161, 393–400. http://dx.doi.org/10.1016/j.jsb.2007.09.014.

Koster, A.J., Grimm, R., Typke, D., Hegerl, R., Stoschek, A., Walz, J., Baumeister, W., 1997. Perspectives of molecular and cellular electron tomography. J. Struct. Biol. 120, 276–308. http://dx.doi.org/10.1006/jsbi.1997.3933.

Kremer, J.R., Mastronarde, D.N., McIntosh, J.R., 1996. Computer visualization of three-dimensional image data using IMOD. J. Struct. Biol. 116, 71–76. http://dx.doi.org/10.1006/jsbi.1996.0013.

Kudryashev, M., Cyrklaff, M., Wallich, R., Baumeister, W., Frischknecht, F., 2010. Distinct in situ structures of the *Borrelia* flagellar motor. J. Struct. Biol. 169, 54–61. http://dx.doi.org/10.1016/j.jsb.2009.08.008.

Kürner, J., Frangakis, A.S., Baumeister, W., 2005. Cryo-electron tomography reveals the cytoskeletal structure of *Spiroplasma melliferum*. Science 307, 436–438. http://dx.doi.org/10.1126/science.1104031.

Liu, J., Lin, T., Botkin, D.J., McCrum, E., Winkler, H., Norris, S.J., 2009. Intact flagellar motor of *Borrelia burgdorferi* revealed by cryo-electron tomography: evidence for stator ring curvature and rotor/C-ring assembly flexion. J. Bacteriol. 191, 5026–5036. http://dx.doi.org/10.1128/JB.00340-09.

Li, Z., Jensen, G.J., 2009. Electron cryotomography: a new view into microbial ultrastructure. Curr. Opin. Microbiol. 12, 333–340. http://dx.doi.org/10.1016/j.mib.2009.03.007.

Li, Z., Trimble, M.J., Brun, Y.V., Jensen, G.J., 2007. The structure of FtsZ filaments in vivo suggests a force-generating role in cell division. EMBO J. 26, 4694–4708. http://dx.doi.org/10.1038/sj.emboj.7601895.

Marko, M., Hsieh, C., Moberlychan, W., Mannella, C.A., Frank, J., 2006. Focused ion beam milling of vitreous water: prospects for an alternative to cryo-ultramicrotomy of frozen-hydrated biological samples. J. Microsc. 222, 42–47. http://dx.doi.org/10.1111/j.1365-2818.2006.01567.x.

McDowall, A.W., Chang, J.J., Freeman, R., Lepault, J., Walter, C.A., Dubochet, J., 1983. Electron microscopy of frozen hydrated sections of vitreous ice and vitrified biological samples. J. Microsc. 131, 1–9.

Milne, J.L.S., Borgnia, M.J., Bartesaghi, A., Tran, E.E.H., Earl, L.A., Schauder, D.M., Lengyel, J., Pierson, J., Patwardhan, A., Subramaniam, S., 2013. Cryo-electron microscopy: a primer for the non-microscopist. FEBS J. 280, 28–45. http://dx.doi.org/10.1111/febs.12078.

Milne, J.L.S., Subramaniam, S., 2009. Cryo-electron tomography of bacteria: progress, challenges and future prospects. Nat. Rev. Microbiol. 7, 666–675. http://dx.doi.org/10.1038/nrmicro2183.

Moissl, C., Rachel, R., Briegel, A., Engelhardt, H., Huber, R., 2005. The unique structure of archaeal "hami", highly complex cell appendages with nano-grappling hooks. Mol. Microbiol. 56, 361–370. http://dx.doi.org/10.1111/j.1365-2958.2005.04294.x.

Murphy, G.E., Matson, E.G., Leadbetter, J.R., Berg, H.C., Jensen, G.J., 2008. Novel ultrastructures of *Treponema primitia* and their implications for motility. Mol. Microbiol. 67, 1184–1195. http://dx.doi.org/10.1111/j.1365-2958.2008.06120.x.

Niederman, R.A., 2006. Structure, function and formation of bacterial intracytoplasmic membranes. In: Shively, J.M. (Ed.), Complex intracellular structures in prokaryotes, Microbiology Monographs. Springer, Heidelberg, Berlin, pp. 193–227.

Pierson, J., Fernández, J.J., Bos, E., Amini, S., Gnaegi, H., Vos, M., Bel, B., Adolfsen, F., Carrascosa, J.L., Peters, P.J., 2010. Improving the technique of vitreous cryo-sectioning for cryo-electron tomography: electrostatic charging for section attachment and implementation of an anti-contamination glove box. J. Struct. Biol. 169, 219–225. http://dx.doi.org/10.1016/j.jsb.2009.10.001.

Pierson, J., Vos, M., McIntosh, J.R., Peters, P.J., 2011. Perspectives on electron cryo-tomography of vitreous cryo-sections. J. Electron. Microsc. (Tokyo) 60 (Suppl 1), S93–S100. http://dx.doi.org/10.1093/jmicro/dfr014.

Pilhofer, M., Ladinsky, M.S., McDowall, A.W., Petroni, G., Jensen, G.J., 2011. Microtubules in bacteria: ancient tubulins build a five-protofilament homolog of the eukaryotic cytoskeleton. PLoS Biol. 9, e1001213. http://dx.doi.org/10.1371/journal.pbio.1001213.

Richter, K., 1994. Cutting artefacts on ultrathin cryosections of biological bulk specimens. Micron Oxford Engl. 1993 (25), 297–308.

Rigort, A., Bäuerlein, F.J.B., Leis, A., Gruska, M., Hoffmann, C., Laugks, T., Böhm, U., Eibauer, M., Gnaegi, H., Baumeister, W., Plitzko, J.M., 2010. Micromachining tools and correlative approaches for cellular cryo-electron tomography. J. Struct. Biol. 172, 169–179. http://dx.doi.org/10.1016/j.jsb.2010.02.011.

Salje, J., Zuber, B., Löwe, J., 2009. Electron cryomicroscopy of *E. coli* reveals filament bundles involved in plasmid DNA segregation. Science 323, 509–512. http://dx.doi.org/10.1126/science.1164346.

Sani, M., Houben, E.N.G., Geurtsen, J., Pierson, J., de Punder, K., van Zon, M., Wever, B., Piersma, S.R., Jiménez, C.R., Daffé, M., Appelmelk, B.J., Bitter, W., van der Wel, N., Peters, P.J., 2010. Direct visualization by cryo-EM of the mycobacterial capsular layer: a labile structure containing ESX-1-secreted proteins. PLoS Pathog. 6, e1000794. http://dx.doi.org/10.1371/journal.ppat.1000794.

Scheffel, A., Gruska, M., Faivre, D., Linaroudis, A., Plitzko, J.M., Schüler, D., 2006. An acidic protein aligns magnetosomes along a filamentous structure in magnetotactic bacteria. Nature 440, 110–114. http://dx.doi.org/10.1038/nature04382.

Shetty, A., Chen, S., Tocheva, E.I., Jensen, G.J., Hickey, W.J., 2011. Nanopods: a new bacterial structure and mechanism for deployment of outer membrane vesicles. PLoS ONE 6, e20725. http://dx.doi.org/10.1371/journal.pone.0020725.

Studer, D., Humbel, B.M., Chiquet, M., 2008. Electron microscopy of high pressure frozen samples: bridging the gap between cellular ultrastructure and atomic resolution. Histochem. Cell Biol. 130, 877–889. http://dx.doi.org/10.1007/s00418-008-0500-1.

Tocheva, E.I., Li, Z., Jensen, G.J., 2010. Electron cryotomography. Cold Spring Harb. Perspect. Biol. 2. http://dx.doi.org/10.1101/cshperspect.a003442.

Toso, D.B., Henstra, A.M., Gunsalus, R.P., Zhou, Z.H., 2011. Structural, mass and elemental analyses of storage granules in methanogenic archaeal cells. Environ. Microbiol. 13, 2587–2599. http://dx.doi.org/10.1111/j.1462-2920.2011.02531.x.

Villa, E., Schaffer, M., Plitzko, J.M., Baumeister, W., 2013. Opening windows into the cell: focused-ion-beam milling for cryo-electron tomography. Curr. Opin. Struct. Biol. 23, 771–777. http://dx.doi.org/10.1016/j.sbi.2013.08.006.

Wikström, M., Kelly, A.A., Georgiev, A., Eriksson, H.M., Klement, M.R., Bogdanov, M., Dowhan, W., Wieslander, A., 2009. Lipid-engineered *Escherichia coli* membranes reveal critical lipid headgroup size for protein function. J. Biol. Chem. 284, 954–965. http://dx.doi.org/10.1074/jbc.M804482200.

Zhang, P., Khursigara, C.M., Hartnell, L.M., Subramaniam, S., 2007. Direct visualization of *Escherichia coli* chemotaxis receptor arrays using cryo-electron microscopy. Proc. Natl. Acad. Sci. U.S.A. 104, 3777–3781. http://dx.doi.org/10.1073/pnas.0610106104.

Zuber, B., Chami, M., Houssin, C., Dubochet, J., Griffiths, G., Daffé, M., 2008. Direct visualization of the outer membrane of mycobacteria and corynebacteria in their native state. J. Bacteriol. 190, 5672–5680. http://dx.doi.org/10.1128/JB.01919-07.